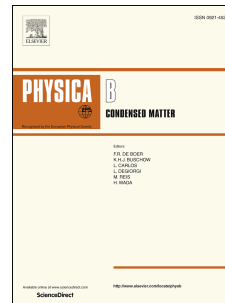# Journal Pre-proof

Evaluation of band gap energy of TiO$_2$ precipitated from titanium sulphate

Salmon Landi, Jr., Iran Rocha Segundo, Cátia Afonso, Orlando Lima, Jr., Manuel F.M. Costa, Elisabete Freitas, Joaquim Carneiro

Please cite this article as: S. Landi Jr., I.R. Segundo, Cá. Afonso, O. Lima Jr., M.F.M. Costa, E. Freitas, J. Carneiro, Evaluation of band gap energy of TiO$_2$ precipitated from titanium sulphate, *Physica B: Physics of Condensed Matter* (2022), doi: https://doi.org/10.1016/j.physb.2022.414008.

This is a PDF file of an article that has undergone enhancements after acceptance, such as the addition of a cover page and metadata, and formatting for readability, but it is not yet the definitive version of record. This version will undergo additional copyediting, typesetting and review before it is published in its final form, but we are providing this version to give early visibility of the article. Please note that, during the production process, errors may be discovered which could affect the content, and all legal disclaimers that apply to the journal pertain.

Evaluation of band gap energy of TiO$_2$ precipitated from titanium sulphate

Salmon Landi Jr.[a,*], Iran Rocha Segundo[b,c], Cátia Afonso[c], Orlando Lima Jr.[b], Manuel F. M. Costa[d], Elisabete Freitas[b] and Joaquim Carneiro[c]

[a]Federal Institute of Education, Science and Technology Goiano, Rio Verde - GO, 75901-970, Brazil
[b]ISISE, Department of Civil Engineering, University of Minho, 4800-058, Guimarães, Portugal
[c]Centre of Physics of Minho and Porto Universities, University of Minho, Azurém Campus, 4800-058, Guimarães, Portugal
[d]Centre of Physics of Minho and Porto Universities, University of Minho, Gualtar Campus, 4710-057, Braga, Portugal

*Correspondence: salmon.landi@ifgoiano.edu.br

Abstract: The determination of the band gap energy (E_g) of semiconductors powder materials can be performed from diffuse reflectance spectroscopy (DRS) measurements. For this purpose, the classical theory proposed by Kubelka and Munk (K-M) and the so-called plot Tauc, both discussed here, have been largely employed. We investigate the E_g values of anatase TiO$_2$ particles synthesized by precipitation of titanyl sulphate in the presence of 5% ammonia solution and titanium and iron salts. Based on K-M function and Tauc plot and considering that the TiO$_2$ anatase phase is an indirect band gap semiconductor, our results indicate that the samples subjected to a mechanochemical treatment (mill rotation speed equal to 300 rpm) present substantially lower E_g values compared to those reported by other authors in a recent work.

Keywords: Band gap energy; Kubelka-Munk function; Tauc plot

1. Introduction

Nowadays, TiO$_2$ is a widely investigated material in diverse studies involving environmental remediation [1,2] and also photovoltaic (PV) devices such as PV solar cells [3,4]. It is well known that the TiO$_2$ non-absorption in the visible region of the electromagnetic spectrum, due to its wide optical band gap energy (E_g), and the recombination ability of electron/hole (e^-/h^+) pairs that are generated during the irradiation process are inherent problems associated with this semiconductor material [5]. However, in order to develop and apply TiO$_2$-based photocatalytic systems in a real context, that is, beyond research laboratories, it is essential that this semiconductor material could efficiently harness solar energy. [6]. In this sense, there are currently different methods, namely, doping, supporting and semiconductor coupling, which have been explored to obtain high photoactive TiO$_2$ under visible irradiation [7].

Regarding the optical characterization of materials, UV-vis diffuse Reflectance Spectroscopy (DRS) is widely used technique to investigate the absorption of light by amorphous and polycrystalline materials [8]. For this propose, a plethora of studies have used the Kubelka-Munk (K-M) model and Tauc plot to determine the E_g of semiconductor materials in the form of powders (non-single-crystal) [9–11].

In a recent article [12], the optical properties of TiO$_2$ particles were investigated from DRS measurements. The aforementioned article states (Section 3.4) that the E_g values were determined directly from the K-M function plotted as a function of the incident photon wavelength (Fig. 5b in that article). It is important to emphasize that this procedure, which ignores the nature of electronic transition between the valence and conduction bands in obtaining E_g, is not the more suitable one as demonstrated by López and Goméz [13]. Therefore,

49 the main goal of this work is to discuss the appropriate method to obtain E_g [14–17] and
50 compare the newly calculated values with those presented by Kucio et al. [12].

51 **2. Methods**

52 **2.1. Tauc Plot**

53   The E_g value of semiconductor materials can be estimated by using the so-called Tauc
54 plot method, which is based on the following equation:

$$\alpha(E) \propto \frac{\left(E - E_g\right)^p}{E}.$$

(1)

55 In Eq. (1), α and E are the absorption coefficient (defined as the probability of light being
56 absorbed per unit path length) and incident photon energy, respectively [18]. The p value
57 depends on the semiconductor band structure, in which $p = 1/2$ for dipole-allowed transitions
58 occurring at a direct band gap and $p = 2$ for dipole-allowed transitions near an indirect gap.
59 Besides that, there are also relevant cases of dipole-forbidden transitions (direct gap $p = 3/2$
60 and indirect gap $p = 3$), where the dipolar transitions are suppressed.
61   It is clear from Eq. (1) that the E_g can be obtained by extrapolating to zero a linear fit of
62 the plot of $(\alpha \times E)^{1/p}$ as a function of E, the so-called Tauc plot [19]. Eq. (1) has often been
63 mistakenly referred to as Tauc's relation/equation/formula [20–22]. However, it should be
64 highlighted that this classical relationship from the theory of optical transitions in
65 semiconductors was not originally derived by Tauc [23].

66 **2.2. Kubelka-Munk model**

67   The description of the diffuse reflectance phenomenon can be realized from a two-flux
68 model based on a differential [24] or integral formulation [25]. Inspired by the work of Schuster
69 [26], Kubelka and Munk proposed differential equations to describe changes in the light
70 intensity traveling through a material medium (of thickness L) deposited on a given substrate
71 (Fig. 1).
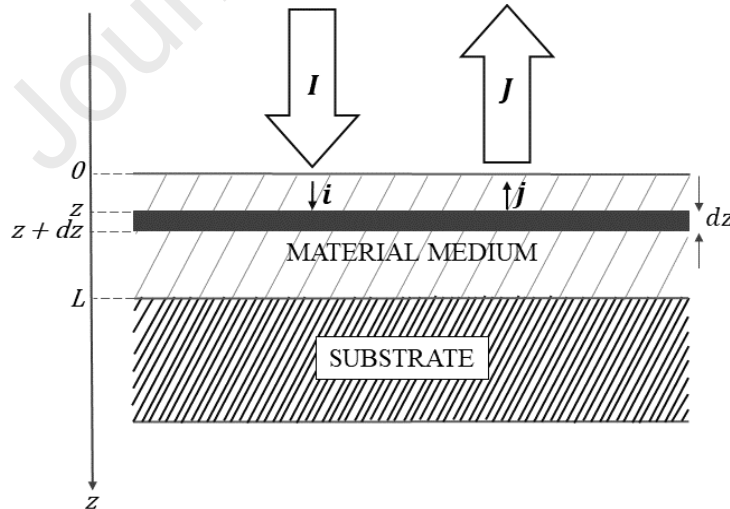
72

73 **Fig. 1:** Diagram for a two-flux diffuse reflectance model, in which i and j represent the intensity of light
74 traveling inside the sample (with thickness L) towards its unilluminated and illuminated surface,
75 respectively.

76   Assuming the light intensity going downward (i) and going upward (j) at any point z,
77 in which $0 \leq z \leq L$, then the infinitesimal variation of i, represented by di, is due to the:
78   I) absorption by the material located within the volume of thickness dz; here, i
79   suffers a decrease ($di < 0$);

80   II)   scattering of light going downward; di is also negative and,

81   III) scattering of light going upward; in this case, di is positive.

82   After these considerations, the following equation is obtained:

$$di = -Ki dz - Si dz + Sj dz, \qquad (2)$$

83   where K and S are the K-M absorption and scattering coefficients, respectively, both being
84   positive and having inverse length units. Similarly, the Eq. (3) for the change in light intensity
85   going upward can be derived. However, it is important to note that for this case dz is negative,
86   that is:

$$-dj = -Kj dz - Sj dz + Si dz \qquad (3)$$

87   When considering a sample with semi-infinite thickness ($L \rightarrow \infty$), which in practice
88   corresponds to thicknesses greater than 2 mm [27], the resolution of Eqs. (2) and (3) implies:

$$\frac{K}{S} = \frac{(1-R)^2}{2R}, \qquad (4)$$

89   where R, defined by the ratio of the intensity (J) of light reflected by the sample and the
90   intensity (I) of incident light, is a dimensionless quantity called diffuse reflectance ($R = J/I$) and
91    $K/S = F(R)$ is the dimensionless K-M function [24,25].

2.3. Obtaining the E_g from DRS data

93   Actually, the sample's diffuse reflectance is measured by a spectrophotometer
94   (equipped with an integrating sphere device) using some material as a reference, usually
95   polytetrafluoroethylene (PTFE) or barium sulphate ($BaSO_4$) pellets [27]. Besides that, when the
96   K-M scattering coefficient and the material scattering coefficient (defined as the probability of
97   light being scattered per unit path length) are considered as constants, the Eq. (5) is obtained
98   [24].

$$\alpha(E) \propto F(R) \qquad (5)$$

99   Therefore, according to the two previous subsections, the E_g can also be determined
100   from $(F(R) \times E)^{1/p}$ against E. However, Kucio et al. used a different procedure to obtain E_g; in
101   fact, the extrapolation to zero was performed from the plots of $F(R)$ versus E. Consequently, the
102   E_g values presented in [12] are quietly incorrect.

103   In order to determine new values of E_g, the coordinates related to the diffuse reflectance
104   ($axis\ y$) versus wavelength ($axis\ x$) in Fig. 5a [12] were obtained for each wavelength (with an
105   incremental step of 1 nm), by using the WebPlotDigitizer free software. It consists in a semi-
106   automated tool that allows the extraction of underlying numerical data from a variety of plots,
107   including XY coordinates, with high levels of reliability and validity [28].

3. Results and Discussion

109   According to the diffraction pattern shown in Fig. 1 [12], the samples investigated by
110   Kucio and co-authors consist of TiO_2 anatase phase, that is, an indirect band gap semiconductor.
111   Therefore, in Eq. (1), p takes a value equal to 2 and according to the previous section the band
112   gap must be calculated from $(F(R) \times E)^{1/2}$ versus E. In this sense, the coordinates obtained
113   from the WebPlotDigitizer were plotted in Fig. 2a and later used to calculate $(F(R) \times E)^{1/2}$. The
114   change of $F(R) \times E)^{1/2}$ as a function of incident photon energy is shown in Fig. 2b.

115
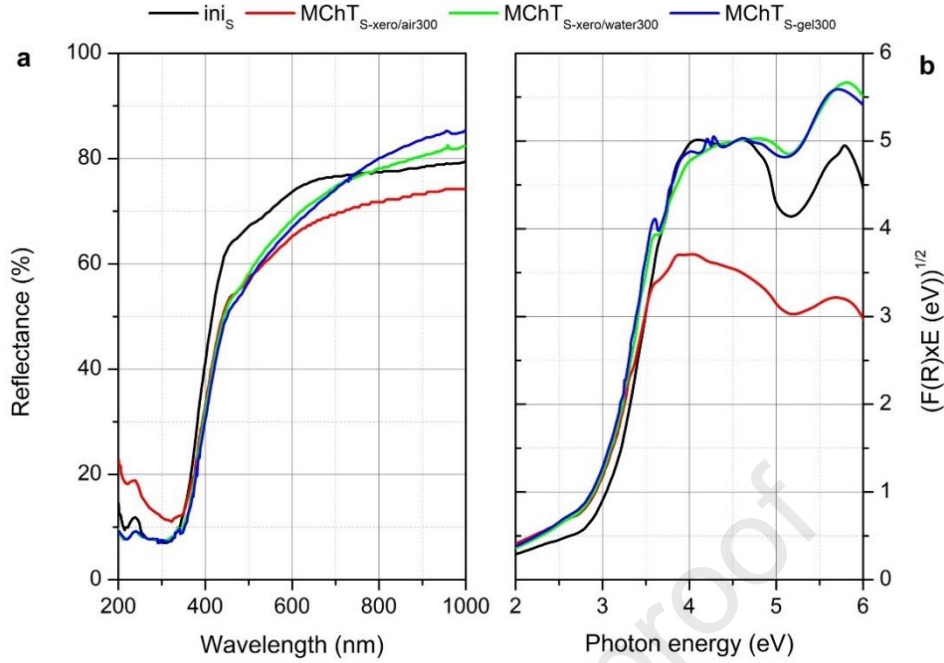
Fig. 2: a) DRS spectra and b) $F(R) \times E)^{1/2}$ corresponding curves.

117   As stated before, from the linear fit of the $F(R) \times E)^{1/2}$ curves shown in Fig. 2b, the new
118   values of E_g were determined. For this purpose, five different intervals were considered, which
119   are located in the region of strong absorption and which present linear behavior in the Tauc plot
120   (Fig. 3).
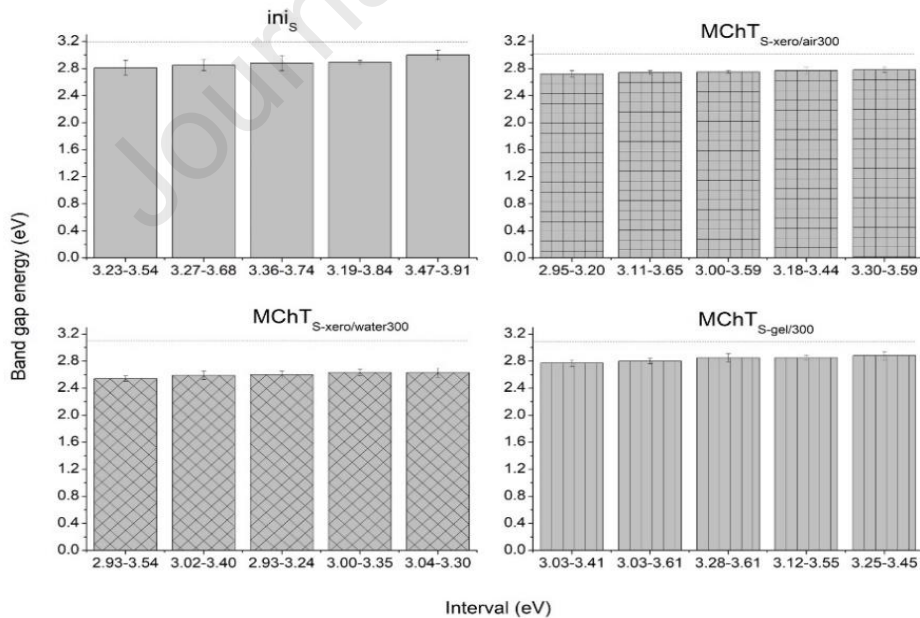
121

122   **Fig. 3:** Indirect band gap values and their respective uncertainties. The E_g values were calculated with the
123   parameters obtained from the linear fits considering different energy intervals (in eV) in Fig. 2b. The
124   dashed lines correspond to the E_g values obtained by Kucio et al. [12].

125   It is important to emphasize that the linear coefficient divided by the slope (in module)
126   of the fit line provides the numerical value of E_g. Therefore, the uncertainty bars in Fig. 3 were

127 determined through diffuse reflectance spectroscopy (DRS) measurements propagation
128 calculations using the quotient' rule. From Fig. 3, it can be observed that, the dashed lines
129 indicate that the E_g values obtained by Kucio et al. [12] are significantly higher than the five
130 values determined in the present work.

131   Table 1 shows the probable range where the E_g value should actually be located (second
132 column) and compares these values with those reported by Kucio et al. [12]. In general, it is well
133 known that the optical properties present some variations that depend on the experimental
134 conditions and chemical composition of the reagents used in the sample synthesis process [29].
135 Anyway, in this work, the band gap energy value for the "ini$_S$" sample was around 3.0 eV,
136 which is in agreement with the value presented by Ola and Maroto-Valer for the anatase phase
137 of TiO$_2$ (without any modification) [30]. Furthermore, it is expected that the other E_g values
138 should also be significantly lower than those presented by Kucio et al., indicating that MChT$_{S-}$
139 $_{xero/air300}$, MChT$_{S-xero/water300}$ and MChT$_{S-gel/300}$ photocatalysts have a wider range of visible light
140 absorption.

141 **Table 1:** Probable range (ΔE) in which the band gap energy value of different TiO$_2$ samples precipitated
142 from titanium sulfate is found compared with those obtained by Kucio et al. [12].

Sample	ΔE (eV)[a]	E_g (eV)[b]
ini$_S$	2.81 – 3.00	3.19
MChT$_{S-xero/air300}$	2.72 – 2.77	3.01
MChT$_{S-xero/water300}$	2.54 – 2.63	3.09
MChT$_{S-gel/300}$	2.77 – 2.88	3.08

143 [a] Minimum and maximum values of E_g calculated using Fig. 2b and the method explained in Section 2.
144 [b] Values presented in [12].

4. Conclusions

146   In this study, the authors revisited the main aspects of the two-flux K-M model and
147 Tauc plot. It was found that Kucio et al used an inappropriate procedure to determine the band
148 gap energy of TiO$_2$ particles from DRS measurements, since they did not take into account that
149 the TiO$_2$ anatase phase is an indirect band gap semiconductor material [12]. Furthermore, in this
150 work, the DRS curves presented in Fig. 5a [12] were obtained by using an image processing
151 software, which enabled the calculation of new band gap energy values from the Tauc plot. Our
152 results show that the samples synthesized by the aforementioned authors are able to absorb
153 visible light even more efficiently, which highlights the importance of the present study for the
154 scientific community.

References

155

156 [1] I. Rocha Segundo, E. Freitas, V.T.F.C. Branco, S. Landi, M.F. Costa, J.O. Carneiro, Review and
157   analysis of advances in functionalized, smart, and multifunctional asphalt mixtures, Renew.
158   Sustain. Energy Rev. 151 (2021) 111552. https://doi.org/10.1016/j.rser.2021.111552.
159 [2] N. Pourshirband, A. Nezamzadeh-Ejhieh, An efficient Z-scheme CdS/g-C$_3$N$_4$ nano catalyst in
160   methyl orange photodegradation: Focus on the scavenging agent and mechanism, J. Mol. Liq. 335
161   (2021) 116543. https://doi.org/10.1016/j.molliq.2021.116543.
162 [3] N. Kanjana, W. Maiaugree, P. Poolcharuansin, P. Laokul, Synthesis and characterization of Fe-
163   doped TiO$_2$ hollow spheres for dye-sensitized solar cell applications, Mater. Sci. Eng. B. 271 (2021)
164   115311. https://doi.org/10.1016/j.mseb.2021.115311.
165 [4] L. Xu, J. Xu, H. Hu, C. Cui, Z. Ding, Y. Yan, P. Lin, P. Wang, Hierarchical submicroflowers
166   assembled from ultrathin anatase TiO2 nanosheets as light scattering centers in TiO$_2$ photoanodes
167   for dye-sensitized solar cells, J. Alloys Compd. 776 (2019) 1002–1008.
168   https://doi.org/10.1016/j.jallcom.2018.10.386.
169 [5] J. Wang, X. Li, Y. Ren, Z. Xia, H. Wang, W. Jiang, C. Liu, S. Zhang, Z. Li, S. Wu, N. Wang, G. Liu, S.
170   Liu, W. Ding, Z. Zhang, The effects of additive on properties of Fe doped TiO$_2$ nanoparticles by
171   modified sol-gel method, J. Alloys Compd. 858 (2021) 157726.
172   https://doi.org/10.1016/j.jallcom.2020.157726.

173 [6] S. Landi Jr., J. Carneiro, P. Parpot, O.S.G.P. Soares, M.F.R. Pereira, A.M. Fonseca, I.C. Neves,
174 Performance of self-cleaning cotton textiles coated with TiO_2, TiO_2-SiO_2 and TiO_2-SiO_2-HY in
175 removing Rhodamine B and Reactive Red 120 dyes from aqueous solutions, Desalin. WATER
176 Treat. 223 (2021) 447–455. https://doi.org/10.5004/dwt.2021.27159.

177 [7] H. Derikvandi, A. Nezamzadeh-Ejhieh, Synergistic effect of p-n heterojunction, supporting and
178 zeolite nanoparticles in enhanced photocatalytic activity of NiO and SnO_2, J. Colloid Interface Sci.
179 490 (2017) 314–327. https://doi.org/10.1016/j.jcis.2016.11.069.

180 [8] F. Soori, A. Nezamzadeh-Ejhieh, Synergistic effects of copper oxide-zeolite nanoparticles
181 composite on photocatalytic degradation of 2,6-dimethylphenol aqueous solution, J. Mol. Liq. 255
182 (2018) 250–256. https://doi.org/10.1016/j.molliq.2018.01.169.

183 [9] N. Pourshirband, A. Nezamzadeh-Ejhieh, S.N. Mirsattari, The CdS/g-C_3N_4 nano-photocatalyst:
184 Brief characterization and kinetic study of photodegradation and mineralization of methyl orange,
185 Spectrochim. Acta Part A Mol. Biomol. Spectrosc. 248 (2021) 119110.
186 https://doi.org/10.1016/j.saa.2020.119110.

187 [10] C.M. Magdalane, G.M.A. Priyadharsini, K. Kaviyarasu, A.I. Jothi, G.G. Simiyon, Synthesis and
188 characterization of TiO_2 doped cobalt ferrite nanoparticles via microwave method: Investigation of
189 photocatalytic performance of congo red degradation dye, Surfaces and Interfaces. 25 (2021)
190 101296. https://doi.org/10.1016/j.surfin.2021.101296.

191 [11] A. Jose, M. John, H. H., S. Kuriakose, B. K.P., T. Varghese, Characterization of $Ce_2(WO_4)_3$
192 nanocrystals for potential applications, Results in Surfaces and Interfaces. 4 (2021) 100020.
193 https://doi.org/10.1016/j.rsurfi.2021.100020.

194 [12] K. Kucio, V. Sydorchuk, S. Khalameida, B. Charmas, The effect of mechanochemical, microwave
195 and hydrothermal modification of precipitated TiO_2 on its physical-chemical and photocatalytic
196 properties, J. Alloys Compd. 862 (2021) 158011. https://doi.org/10.1016/j.jallcom.2020.158011.

197 [13] R. López, R. Gómez, Band-gap energy estimation from diffuse reflectance measurements on sol–
198 gel and commercial TiO_2: a comparative study, J. Sol-Gel Sci. Technol. 61 (2012) 1–7.
199 https://doi.org/10.1007/s10971-011-2582-9.

200 [14] F. Iazdani, A. Nezamzadeh-Ejhieh, FeO-Clinoptilolite nanoparticles: Brief characterization and its
201 photocatalytic kinetics towards 2,4-dichloroaniline, Chem. Phys. 550 (2021) 111305.
202 https://doi.org/10.1016/j.chemphys.2021.111305.

203 [15] V. Medvecká, J. Surovčík, T. Roch, M. Zahoran, D. Pavliňák, D. Kováčik, ZnO nanofibers prepared
204 by plasma assisted calcination: Characterization and photocatalytic properties, Appl. Surf. Sci. 581
205 (2022) 152384. https://doi.org/10.1016/j.apsusc.2021.152384.

206 [16] N. Pourshirband, A. Nezamzadeh-Ejhieh, A Z-scheme AgI/BiOI binary nanophotocatalyst for the
207 Eriochrome Black T photodegradation: A scavenging agents study, Mater. Res. Bull. 148 (2022)
208 111689. https://doi.org/10.1016/j.materresbull.2021.111689.

209 [17] S. Dwivedi, H.C. Nayak, S.S. Parmar, R.P. Kumhar, S. Rajput, Calcination Temperature Reflected
210 Structural, Optical and Magnetic Properties of Nickel Oxide, Magnetism. 2 (2022) 45–55.
211 https://doi.org/10.3390/magnetism2010004.

212 [18] C. Malerba, F. Biccari, C. Leonor Azanza Ricardo, M. D'Incau, P. Scardi, A. Mittiga, Absorption
213 coefficient of bulk and thin film Cu_2O, Sol. Energy Mater. Sol. Cells. 95 (2011) 2848–2854.
214 https://doi.org/10.1016/j.solmat.2011.05.047.

215 [19] A. MURPHY, Band-gap determination from diffuse reflectance measurements of semiconductor
216 films, and application to photoelectrochemical water-splitting, Sol. Energy Mater. Sol. Cells. 91
217 (2007) 1326–1337. https://doi.org/10.1016/j.solmat.2007.05.005.

218 [20] Y. Shao, M. Ji, Y. Zhang, J. Zhao, Z. Liu, H. Li, H. Li, S. Yin, J. Xia, Integration of double halogen
219 atoms in atomically thin bismuth bromide: Mutative electronic structure steering charge carrier
220 migration boosted broad-spectrum photocatalysis, Appl. Surf. Sci. 541 (2021) 148477.
221 https://doi.org/10.1016/j.apsusc.2020.148477.

222 [21] H. Park, N. Son, B.H. Park, S.W. Joo, M. Kang, Visible light-induced stable HER performance
223 using duality of ultrafine Pt NPs in a Z-scheme p-n junction Fe_2O_3@Pt@FeS catalyst, Appl. Surf. Sci.
224 541 (2021) 148347. https://doi.org/10.1016/j.apsusc.2020.148347.

225 [22] L. Wei, J. Zhang, M. Ruan, Combined CdS/In_2S_3 heterostructures with cocatalyst for boosting
226 carriers separation and photoelectrochemical water splitting, Appl. Surf. Sci. 541 (2021) 148431.
227 https://doi.org/10.1016/j.apsusc.2020.148431.

228 [23] S. Landi, Comment on "Photocatalytic degradation of RhB from an aqueous solution using
229 Ag_3PO_4/N-TiO_2 heterostructure" and "Evaluation of the effect of dose change of Fe_3O_4

230   nanoparticles on electrochemical biosensor compatibility using hydrogels as an experimental l, J.
231   Mol. Liq. 338 (2021) 116635. https://doi.org/10.1016/j.molliq.2021.116635.

232   [24]   S. Landi, I.R. Segundo, E. Freitas, M. Vasilevskiy, J. Carneiro, C.J. Tavares, Use and misuse of the
233   Kubelka-Munk function to obtain the band gap energy from diffuse reflectance measurements,
234   Solid State Commun. 341 (2022) 114573. https://doi.org/10.1016/j.ssc.2021.114573.

235   [25]   M.L. Myrick, M.N. Simcock, M. Baranowski, H. Brooke, S.L. Morgan, J.N. McCutcheon, The
236   Kubelka-Munk Diffuse Reflectance Formula Revisited, Appl. Spectrosc. Rev. 46 (2011) 140–165.
237   https://doi.org/10.1080/05704928.2010.537004.

238   [26]   A. Schuster, Radiation Through a Foggy Atmosphere, Astrophys. J. 21 (1905) 1.
239   https://doi.org/10.1086/141186.

240   [27]   A. Escobedo-Morales, I.I. Ruiz-López, M. deL. Ruiz-Peralta, L. Tepech-Carrillo, M. Sánchez-Cantú,
241   J.E. Moreno-Orea, Automated method for the determination of the band gap energy of pure and
242   mixed powder samples using diffuse reflectance spectroscopy, Heliyon. 5 (2019) e01505.
243   https://doi.org/10.1016/j.heliyon.2019.e01505.

244   [28]   D. Drevon, S.R. Fursa, A.L. Malcolm, Intercoder Reliability and Validity of WebPlotDigitizer in
245   Extracting Graphed Data, Behav. Modif. 41 (2017) 323–339.
246   https://doi.org/10.1177/0145445516673998.

247   [29]   P. Kutálek, L. Tichý, On the thickness dependence of both the optical band gap and reversible
248   photodarkening in amorphous Ge-Se films, Thin Solid Films. 619 (2016) 336–341.
249   https://doi.org/10.1016/j.tsf.2016.10.037.

250   [30]   O. Ola, M.M. Maroto-Valer, Transition metal oxide based TiO_2 nanoparticles for visible light
251   induced CO_2 photoreduction, Appl. Catal. A Gen. 502 (2015) 114–121.
252   https://doi.org/10.1016/j.apcata.2015.06.007.

253

Declaration of interests

☒ The authors declare that they have no known competing financial interests or personal relationships that could have appeared to influence the work reported in this paper.

☐The authors declare the following financial interests/personal relationships which may be considered as potential competing interests: